

CLOCK SYNCHRONIZATION USING GPS/GLONASS CARRIER PHASE

K. Y. Tu¹, H. M. Peng¹, C. S. Liao²

National Standard Time & Frequency Lab.,
TL, Chunghwa Telecom Co., Ltd., Taiwan

F. R. Chang³

Dept. of Electrical Engineering, National Taiwan University, Taiwan

¹Associate Researcher

²Senior Researcher

³Professor

Abstract

Clock synchronization by means of GPS/GLONASS is proposed. The GPS/GLONASS receivers with the external frequency input interface are used in our system. While the remote OCXO (Oven-Controlled Crystal Oscillator) clock and the primary H-maser clock are connected to the receivers, the frequency offset of the remote clock with respect to the primary clock can be estimated by performing the linear-least-square fit on carrier-phase single-difference observables. The proportional controller is adopted in our system for tuning the remote clock in real time. Through the D/A converter, the remote clock is then steered to synchronism with the primary clock. For averaging times of 1 day under the configuration of about a 30-meter baseline, our experimental results show that the accuracy of the remote clock can be improved from about 2×10^{-9} to about 6×10^{-14} , and the stability of the remote clock can be improved from about 2×10^{-10} to about a few parts in 10^{14} . Based on the proposed architecture, the frequency traceability can be achieved. The potential applications include a frequency source system for calibration laboratories, telecommunication networks, and power transmission systems.

INTRODUCTION

The capability of using GPS carrier phase to transfer precise time and frequency has been recognized and described by many researchers [6-10]. Because the frequency of the carrier is roughly 1000 times higher than that of C/A code, time and frequency dissemination using carrier phase has much greater resolution, in principle. When combined with Russia's GLONASS constellation, which provides similar capabilities, the potential precision of the system becomes even greater. Recent development in time and frequency applications have led the timekeeping community to focus on using both these systems for time metrology.

In this paper, we propose a scheme for clock synchronization by using GPS/GLONASS carrier phase. The basic architecture of the system is shown in Figure 1. With all-in-view observations, the frequency offset of the remote clock with respect to the primary clock is estimated in real time by performing the linear-least-square fit on carrier-phase single-difference observables over observation period. In the process, the errors and biases that affect the measurements are substantially reduced. In our system, the carrier-phase data and other observation messages are passed between both stations through PSTN (Public Switched-Telephone Network). The frequency offset is then fed into a proportional controller, which automatically issues commands

to steer the remote clock to synchronize with the primary clock. On the other hand, the master station can also monitor the performance of the remote clock in real time.

With the above-mentioned method, the accuracy of the remote OCXO clock could be improved from about 2×10^{-9} to about 6×10^{-14} for average times of one day. The stability of the remote OCXO clock could be improved from about 3×10^{-10} to about 2×10^{-14} . The potential roles of our system include the PRSs for telecommunication networks and the FSs for calibration laboratories, power systems, navigation systems, instrument calibration, and others.

THE MODEL OF CARRIER PHASE OBSERVABLES

In order to combine GPS and GLONASS, a unique time scale for all observations and satellite ephemerides and a unique reference system for all satellite and receiver positions are required. In our approach, all computations is based on GPS time as reference time and referred to the reference frame WGS-84. Therefore, the epochs of the GLONASS ephemerides are approximately corrected to GPS time by applying the leap seconds between GPS time and UTC. The GLONASS satellite positions are transformed from the frame PZ-90 to WGS-84 by applying the transformation parameters given in [3]. The observation equations for both GPS and GLONASS systems may also be modeled as Equation (1) [1-2], provided the corresponding carrier frequencies are introduced. In the processing of combined GLONASS/GPS observations, the differences between GPS and GLONASS frequencies and the wavelengths for GPS/GLONASS satellite pairs need to be considered, however.

$$\Phi_A^j = \rho_A^j + c(dt^j - dT_A) + \lambda^j N_A^j - d_{ion}^j + d_{trop}^j + \varepsilon_A^j, \quad (1)$$

where Φ_A^j is the carrier-phase measurement of the receiver A from the satellite j in meter; ρ_A^j is the true distance between the receiver A and the satellite j ; c is the speed of light; dt^j is the clock bias of the satellite j ; dT_A represents the clock difference between the satellite system time and receiver A clock; λ^j is nominal wavelength of the signal from satellite j ; N_A^j denotes the unknown integer number of cycles (ambiguity); and d_{ion}^j and d_{trop}^j are the ionospheric delay and the tropospheric delay, respectively; ε_A^j is the unmodeled errors primarily due to multipath, temperature variation, physical factors, etc.

To study the clock synchronization, we would like to first examine the behavior of the oscillator. Hence, both of the remote clock and primary clock are connected to the GNSS receivers, respectively. Under this arrangement, the term dT_A in (1) represents the time difference between the satellite clock and the external clock A . Denoting the two receivers by A and B and the satellite by j , respectively, the single-difference equation is

$$\Delta\phi_{AB}^j = \Delta\rho_{AB}^j - c\Delta dT_{AB} + \lambda^j \Delta N_{AB}^j + \Delta\varepsilon_{AB}^j, \quad (2)$$

where $\Delta(\cdot)$ represents the operator for differences between receivers with the same satellite. Due to the strong correlation between the unmodeled ionospheric and tropospheric delays of the

two receivers over a short baseline, the terms d_{ion}^j and d_{hop}^j in (1) are then eliminated. Since dT_A and dT_B are both referring to the same satellite system clock, their difference ΔdT_{AB} in (2) is nothing but the phase difference between external clock A and external clock B .

SYSTEM ARCHITECTURE

Figure 3 shows the functional block diagram of our system. It consists of the master station and the remote station. The master station contains the hydrogen-maser clock, GNSS receiver, and PC. The remote station includes the low-cost OCXO, GNSS receiver, D/A converter and industrial PC. Through the wired or wireless data links, the carrier-phase data and other observation messages can be sent between both stations. The positions of the antennae are predetermined by IGS (International GPS Service), and the j -th GPS and GLONASS satellite positions are obtained from the broadcasting navigation messages.

By performing the linear-least-square fit on the carrier-phase single-difference model (2) over observation interval τ , we can estimate the frequency offset y_τ of the remote clock with respect to the primary clock. With all-in-view GPS/GLONASS observations, the integrated frequency offset \bar{y}_τ then can be obtained by weighted averaging y_τ .

In general, the fine frequency tuning can be performed on the inexpensive oscillator through voltage control. Because of environmental effects such as vibration, temperature, pressure, and humidity, the desired frequency output is not always under a constant voltage. In our system, the frequency offset \bar{y}_τ is chosen as the input variables of the controllers. An incremental voltage $\Delta V(t_i)$ will be generated to update the voltage for steering the oscillator.

$$V_{i+1} = V_i + \Delta V. \quad (3)$$

In our system, we considered the proportional control [4] in the remote clock. The block diagram for the controller used in our experiment is shown in Figure 3. The control signal is proportional to the frequency offset \bar{y}_τ with gain K being adjustable. To design a particular control loop for the clock synchronization applications, we merely have to adjust the constants K in Figure 3 to achieve an acceptable level of performance. With some trial and error, the gain K is determined.

EXPERIMENTAL RESULTS

The basic experimental structure for tests is shown in Figure 2. In the master station, the 5 MHz of the hydrogen clock used as primary clock was connected to a Ashtech™ GG-24 receiver. The OCXO manufactured by Datum™, Model FTS 1130, was used as the remote clock. The carrier-phase data and other observation messages were passed between both stations through the PSTN interface.

In our experiment, the software, including the proportional controller, communication interface, and data collection, were programmed in C++ on Windows® 2000 and executed on an industrial

PC manufactured by ADVANTECHTM. The data used for the frequency accuracy and stability analysis were measured every 1 second by a TIC (Time Interval Counter) manufactured by SRSTM, model SR620.

For the stability analysis of frequency source under tests, we made use of the IEEE recommended MDEV (Modified Allan Deviation) [11], which is a standard practice in the time and frequency community. In our experiment, the confidence intervals applied to the frequency stability analysis were set to $\pm 68\%$.

We examined the performance of free-running OCXO used in our system and the OCXO under control. These frequency analyses are shown in Figure 4. The OCXO line in Figure 4 shows the frequency instability. The OCXO-C line shows the typical results of frequency stability analyses of the remote OCXO clock under control. These results reveal the high frequency stability of the remote clock not only over the short term, but also over the long term. The frequency stability of the OCXO clock could be improved from about 3×10^{-10} to about 2×10^{-14} for average times of 1 day.

In addition, to assess the limitations of our system regarding clock synchronization, we conducted an experiment by connecting a common hydrogen-maser clock to GNSS receivers in both stations over about a 30-meter baseline. The results of the frequency stability analyses are shown in Figure 5. These results show that our system has a very high frequency stability of about 2×10^{-15} for averaging times of one day.

Figure 6 shows the phase differences between the free-running OCXO clock and the primary clock. The accuracy of this OCXO is about 2.3×10^{-9} for average times of 1 day. Over the approximately 30-meter baseline, the remote OCXO clock is automatically steered to approach synchronization with the primary clock. The accuracy of the remote OCXO clock can be improved from about 2.3×10^{-9} to 5.49×10^{-14} for averaging times of 1 day.

CONCLUSIONS

A new scheme for clock synchronization by using GPS/GLONASS carrier phase is presented. Experimental results show that combining GPS and GLONASS carrier phase seems to provide definite additional value for frequency dissemination. In the experiments, the low-cost OCXO clock could be automatically steered to obtain the very high frequency accuracy and stability in the short term as well as in the long term. In addition, the proposed architecture can achieve the traceability of frequency dissemination. At present, we are trying to establish the frequency source for calibration laboratories and telecommunication networks based on the proposed scheme in Taiwan.

ACKNOWLEDGMENT

We gratefully acknowledge the NBS (National Bureau of Standards) of the R.O.C. for supporting this project.

REFERENCES

- [1] B. Hofmann-Wellenhof, H. Lichtenegger, and J. Collins, *Global Positioning System Theory and Practice*, Springer-Verlag Wien, New York, USA, 1994.
- [2] D. Wells, *Guide to GPS Positioning*, Canadian GPS Associates, 1996.
- [3] von H. Habrich, *Geodetic Applications of the Global Navigation Satellite System (GLONASS) and of GLONASS/GPS Combinations*, 2000
- [4] G. F. Franklin, J. D. Powell and A. Emami-Naeini, *Feedback Control of Dynamic Systems*, 3rd ed. MA: Addison-Wesley, 1994.
- [5] J. A. Davis and J. M. Furlong, *Report on the study to determine the suitability of GPS disciplined oscillators as time and frequency standards traceable to the UK national time scale UTC(NPL)*, Centre for Time Metrology, National Physical Laboratory, UK, 1997.
- [6] G. Petit and C. Thomas, "GPS frequency transfer using carrier-phase measurements," *Proc IEEE Freq. Contr Symp.*, pp. 1151-1159, 1996.
- [7] K. Larson, and J. Levine, "Time-transfer using GPS Carrier Phase Methods", *Proc 29th the Precise Time and Time Interval Meeting*, Long Beach, California, 1997.
- [8] C. Bruyninx, P. Defraigne, J. M. Sleewaegen, and P. Paquet, "Frequency transfer using GPS: comparative study of code and carrier phase analysis results," *Proc 30th Precise Time and Time Interval Meeting*, 1998.
- [9] D. Jefferson, S. Linchten, and L. Young, "A test of precision GPS clock synchronization," *Proc IEEE Freq. Contr Symp.*, pp. 1206-1210, 1996.
- [10] D. Allan and M. Weiss, "Accurate time and frequency transfer using common-view of a GPS satellite," *Proc IEEE Freq. Contr Symp.*, pp. 334-356, 1998.
- [11] International Telecommunication Union Telecommunication Standardization Sector (ITU-T), G. 810, "Definitions and terminology for synchronization," Aug. 1996.
- [12] International Telecommunication Union Telecommunication Standardization Sector (ITU-T), G.811, "Timing characteristics of primary reference clocks," Sept. 1997.

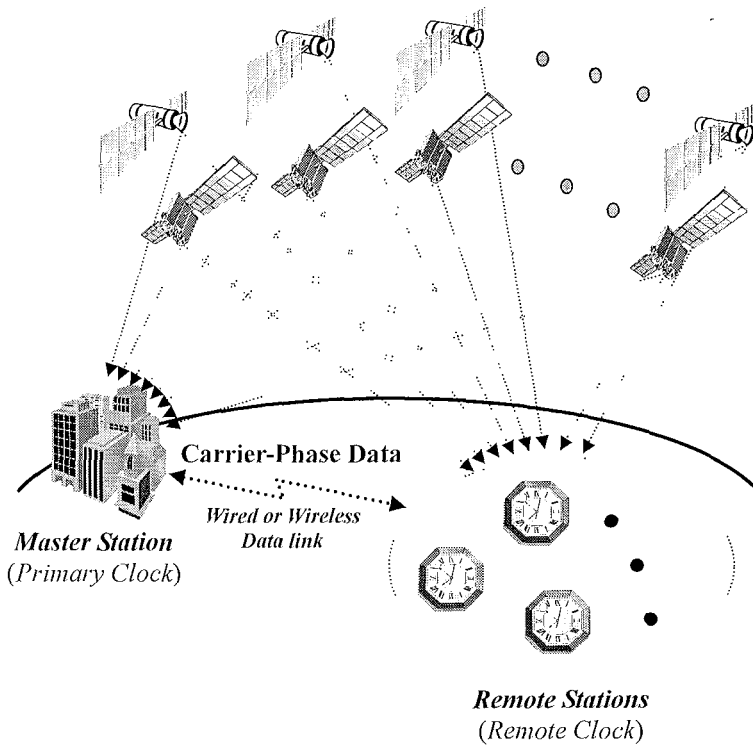


Figure 1. The system architecture for the clock synchronization by using GPS/GLONASS carrier-phase measurements.

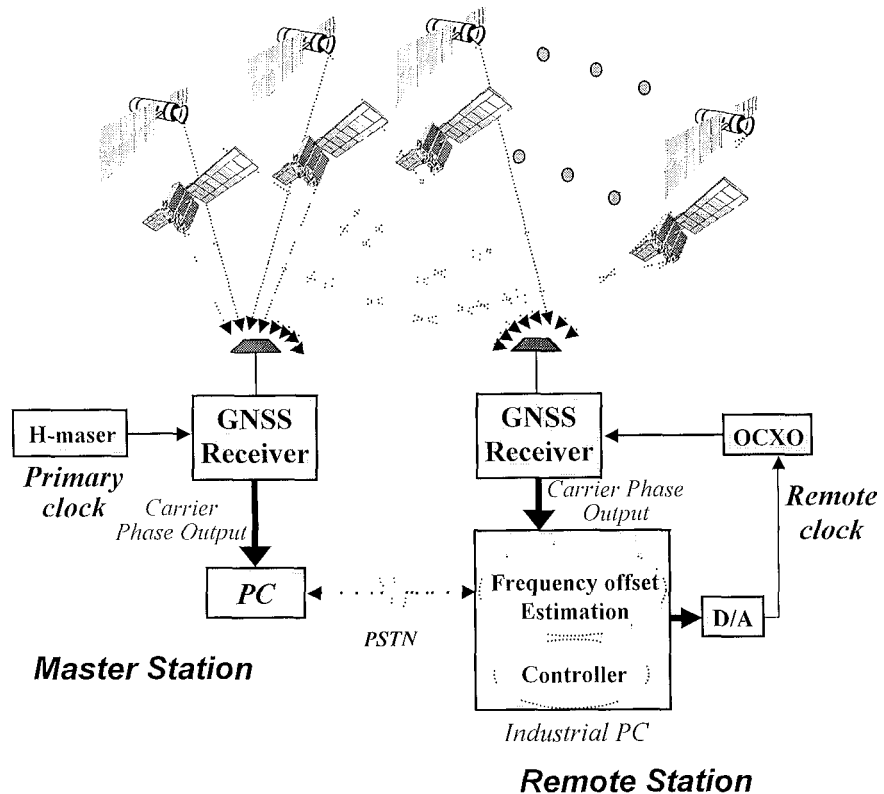


Figure 2. The functional block diagram for the clock synchronization by using GPS/GLONASS carrier-phase measurements.

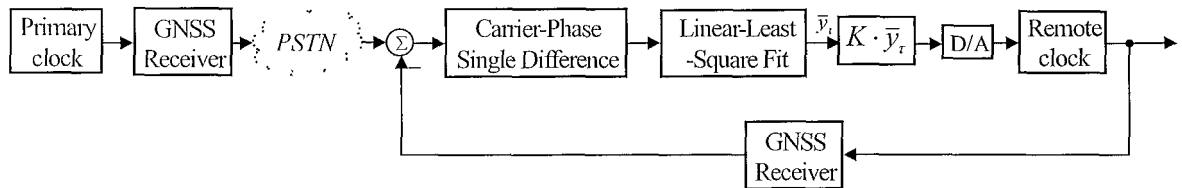


Figure 3. Control block diagram.

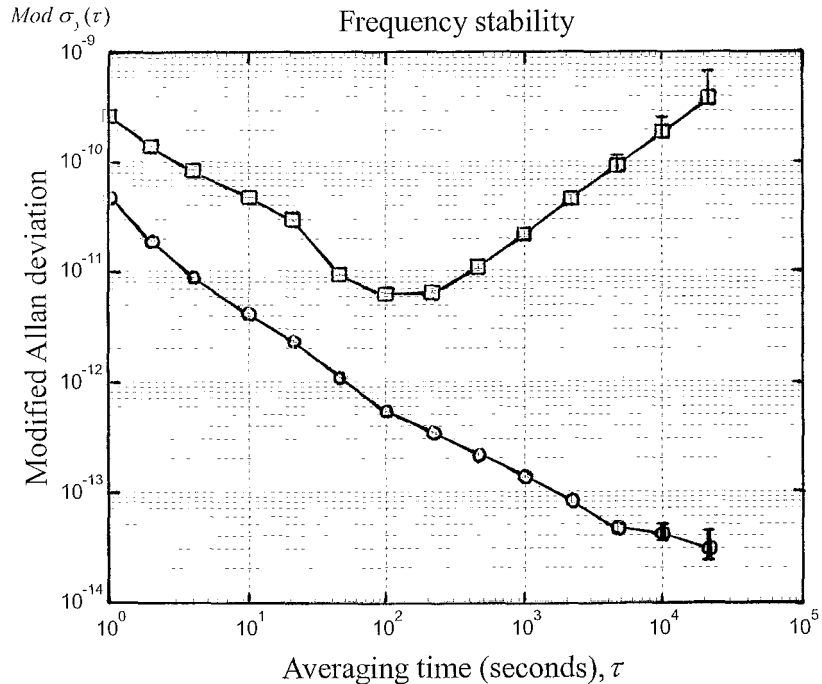


Figure 4. The frequency stability analysis of the free running OCXO (OCXO line) and the OCXO under control (OCXO-C line).

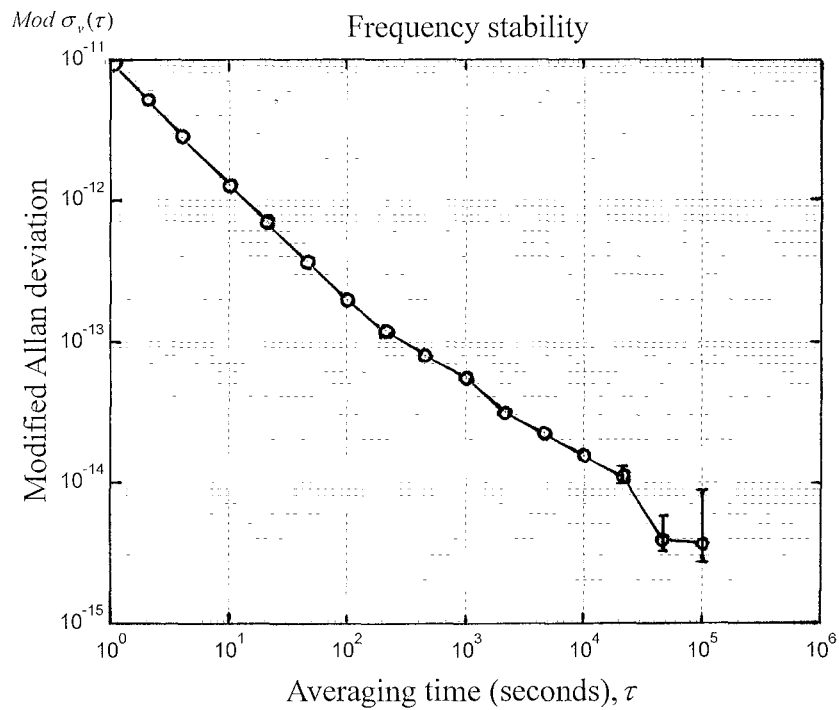


Figure 5. The frequency stability analysis of our system by using the common H-maser clock over short baseline.

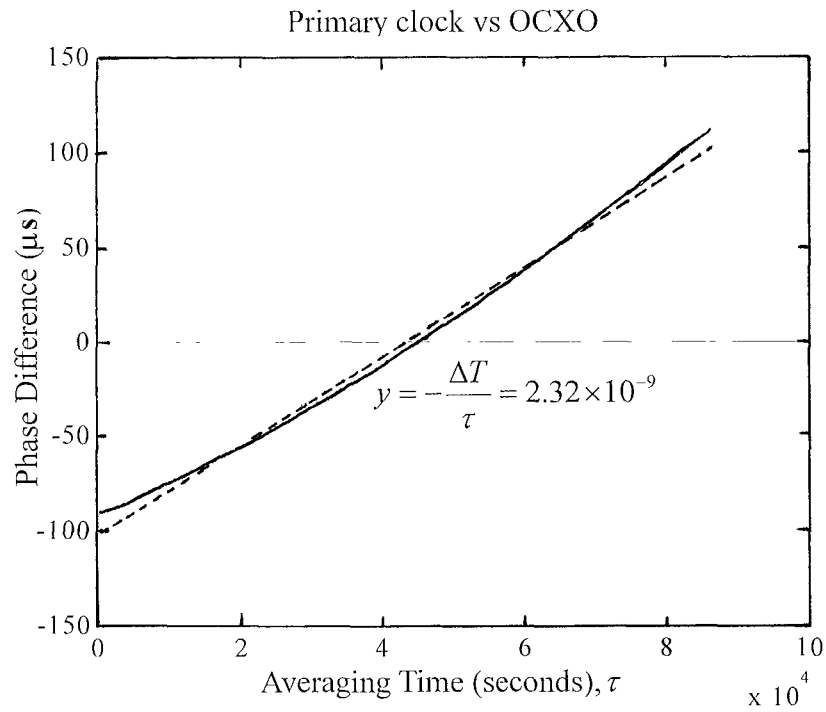


Figure 6 Phase difference between free-running OCXO and primary clock with linear-fit line.

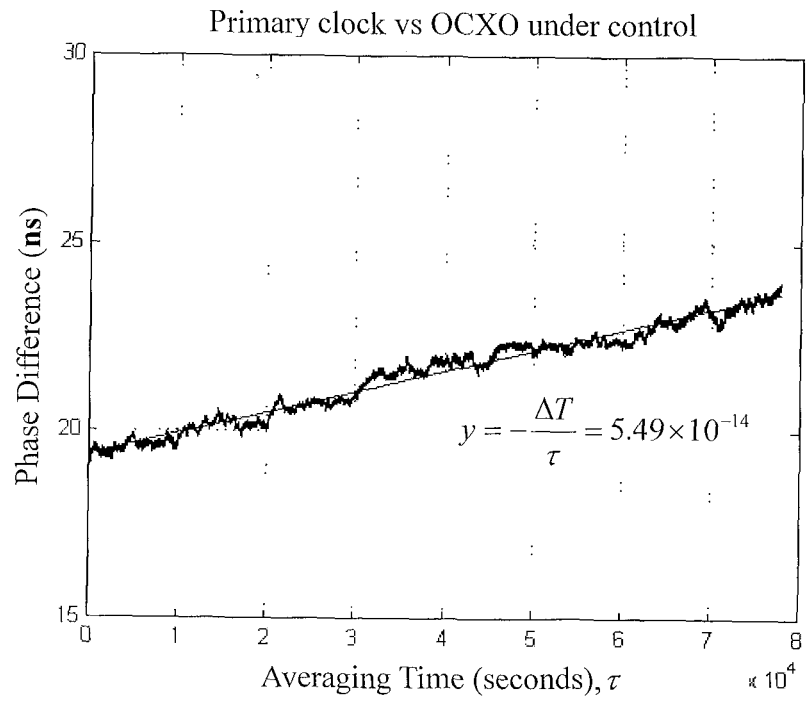


Figure 7. Phase difference between primary clock and remote OCXO clock under control with linear-fit line.